Biophysical Letter

Ensemble-Biased Metadynamics: A Molecular Simulation Method to Sample Experimental Distributions

Fabrizio Marinelli[1,*] and José D. Faraldo-Gómez[1,*]
[1]Theoretical Molecular Biophysics Section, National Heart, Lung and Blood Institute, National Institutes of Health, Bethesda, Maryland

ABSTRACT We introduce an enhanced-sampling method for molecular dynamics (MD) simulations referred to as ensemble-biased metadynamics (EBMetaD). The method biases a conventional MD simulation to sample a molecular ensemble that is consistent with one or more probability distributions known a priori, e.g., experimental intramolecular distance distributions obtained by double electron-electron resonance or other spectroscopic techniques. To this end, EBMetaD adds an adaptive biasing potential throughout the simulation that discourages sampling of configurations inconsistent with the target probability distributions. The bias introduced is the minimum necessary to fulfill the target distributions, i.e., EBMetaD satisfies the maximum-entropy principle. Unlike other methods, EBMetaD does not require multiple simulation replicas or the introduction of Lagrange multipliers, and is therefore computationally efficient and straightforward in practice. We demonstrate the performance and accuracy of the method for a model system as well as for spin-labeled T4 lysozyme in explicit water, and show how EBMetaD reproduces three double electron-electron resonance distance distributions concurrently within a few tens of nanoseconds of simulation time. EBMetaD is integrated in the open-source PLUMED plug-in (www.plumed-code.org), and can be therefore readily used with multiple MD engines.

Received for publication 1 April 2015 and in final form 20 May 2015.

*Correspondence: fabrizio.marinelli@nih.gov or jose.faraldo@nih.gov

Biophysical techniques probing the structural dynamics of biomolecules typically yield signals that arise from an ensemble of molecular conformations, and thus it is often not straightforward to interpret the experimental data unambiguously. For example, double electron-electron resonance (DEER) spectroscopy is increasingly used to measure distances between spin-labeled cysteine residues (1), and to assess conformational mechanisms in proteins. DEER spectra, however, actually translate into distance probability distributions, which are often multimodal and interdependent, and might reflect a variety of protein conformations and rotameric states of the labels.

Molecular dynamics (MD) simulations are arguably the best computational approach to address this problem. The concept is to employ an MD simulation to construct an ensemble of molecular configurations $\mathbf{X}$ that is consistent with the measured probability distribution of an observable $\xi = \xi^f(\mathbf{X})$, while simultaneously representing the molecular system more realistically (solvent, temperature, etc.) than in standard structural-refinement methods. In practice, this approach entails a modification of the simulation energy function, $U(\mathbf{X})$, so that the resulting probability distribution, $\rho(\mathbf{X})$, fulfills the experimental data with the minimum possible bias i.e., the so-called maximum-entropy principle (2,3). If the experimental data for observable ξ is binned into a histogram, a possible modification of $U(\mathbf{X})$ is a linear perturbation, leading to (4)

$$\rho(\mathbf{X}) = \frac{\exp\{-\beta\, U(\mathbf{X}) + \sum_i \lambda_i h_i[\xi^f(\mathbf{X})]\}}{\int d\mathbf{X}'\, \exp\{-\beta U(\mathbf{X}') + \sum_i \lambda_i h_i[\xi^f(\mathbf{X}')]\}}, \quad (1)$$

where the i index denotes each of the bins in the measured histogram of ξ, and $h_i[\xi^f(\mathbf{X})] = 1$ if the value of $\xi^f(\mathbf{X})$ is in bin i, while $h_i[\xi^f(\mathbf{X})] = 0$ otherwise (and $\beta = 1/k_B T$, where k_B is the Boltzmann constant and T is the temperature). The λ_i parameters, which must be determined in each case, ensure that the time averages of $h_i(\xi^f(\mathbf{X}))$ are equal to the experimental probability values for each of the bins i. Practical applications of the maximum-entropy formulation in Eq. 1 have so far relied on computationally intensive approaches such as averaging over multiple system replicas simulated concurrently (4–7) or iterative optimization algorithms to determine the values of λ_i (2,3).

Here, we present an alternative, single-replica approach inspired by the metadynamics method (8,9), which is also consistent with the maximum-entropy principle. We refer to this method as ensemble-biased metadynamics (EBMetaD). Let us define $\rho_{exp}(\xi)$ as the target experimental probability distribution of observable ξ and $F(\xi)$ as the free energy,

Editor: Bert de Groot.

http://dx.doi.org/10.1016/j.bpj.2015.05.024

$$F(\xi) = -\frac{1}{\beta}\ln\left[\int d\mathbf{X}\,\exp\{-\beta U(\mathbf{X})\}\delta\left(\xi - \xi^f(\mathbf{X})\right)\right] + C, \tag{2}$$

where C is a constant. In the limit of infinitesimally narrow bins, Eq. 1 becomes (Appendix S1 in the Supporting Material):

$$\rho(\mathbf{X}) = \frac{\exp\{-\beta U(\mathbf{X}) + \ln\rho_{\exp}[\xi^f(\mathbf{X})] + \beta F[\xi^f(\mathbf{X})]\}}{\int dX'\,\exp\{-\beta U(\mathbf{X}') + \ln\rho_{\exp}[\xi^f(\mathbf{X}')] + \beta F[\xi^f(\mathbf{X}')]\}}. \tag{3}$$

In EBMetaD, a biasing potential is added to the energy function so that the simulation samples $\rho(\mathbf{X})$ in Eq. 3. Like in standard metadynamics, this biasing potential, denoted by $V(\xi^f(\mathbf{X}),t)$, is constructed throughout the simulation as a cumulative sum of Gaussians, added one at a time at a frequency of $1/\tau$, each centered on the value of ξ at that time. In EBMetaD, however, these Gaussian functions are weighted by the target probability distribution, that is

$$V(\xi,t) = \sum_{t'=\tau,2\tau\ldots}^{t} \frac{w\,\exp\{-[\xi - \xi^f(\mathbf{X}_{t'})]^2/2\sigma^2\}}{\exp\{S_\rho\}\rho_{\exp}[\xi^f(\mathbf{X}_{t'})]}, \tag{4}$$

where $\mathbf{X}_{t'}$ denotes the atomic coordinates at time t' and σ is the Gaussians width, which sets the resolution of $F(\xi)$ and $\rho_{\exp}(\xi)$. The quantity $S_\rho = -\int d\xi \rho_{\exp}(\xi)\ln[\rho_{\exp}(\xi)]$ is the differential entropy of $\rho_{\exp}(\xi)$, i.e., $\exp\{S_\rho\}$ is the effective volume in ξ spanned by $\rho_{\exp}(\xi)$, and serves a normalization factor to ensure that the mean height of the Gaussians added in the range of $\rho_{\exp}(\xi)$ is equal to w. As in standard metadynamics, EBMetaD simulations remain close to equilibrium if w, σ, and τ in Eq. 4 are selected adequately (Appendix S2 in the Supporting Material), and a stationary condition is reached at a certain time t_e after which the biasing potential fluctuates around an average profile that converges asymptotically (10). Specifically, the change of $V(\xi^f(\mathbf{X}),t)$ from this point forward is (11,12)

$$\dot{V}(\xi, t{>}t_e) \approx \frac{C}{\rho_{\exp}(\xi)} \frac{\exp\{-\beta[F(\xi) + V(\xi,t)]\}}{\int d\xi'\,\exp\{-\beta\,[F(\xi') + V(\xi',t)]\}} \approx C, \tag{5}$$

where C is a constant. Provided that the region in which $\rho_{\exp}(\xi){>}0$ is energetically allowed by $U(\mathbf{X})$, the implication of Eq. 5 is that the average biasing potential converges to

$$\overline{V}(\xi, t{>}t_e) \approx -\frac{1}{\beta}\ln\rho_{\exp}(\xi) - F(\xi). \tag{6}$$

That is, when $t > t_e$, the EBMetaD simulation samples the space of ξ as in the target distribution $\rho_{\exp}(\xi)$.

It is straightforward to generalize this approach to the case of multiple observables ξ_i and probability distributions thereof, $\rho_{\exp}[\xi_i^f(\mathbf{X})]$, employing a multidimensional biasing potential analogous to that in Eq. 4:

$$V(\xi_1,\xi_2,\ldots,t) = \sum_{t'=\tau,2\tau\ldots}^{t}\sum_i \frac{w_i\,\exp\{-[\xi_i - \xi_i^f(\mathbf{X}_{t'})]^2/2\sigma_i^2\}}{\exp\{S_{\rho_i}\}\rho_{\exp}[\xi_i^f(\mathbf{X}_{t'})]}. \tag{7}$$

Owing to the scaling factors S_{ρ_i}, several distributions can be simultaneously targeted even if they have very different effective volumes. The observables ξ_i, however, ought not be a function of each other (2–4).

To test the validity of the EBMetaD method, we first considered the two-dimensional model potential $U(\xi,\xi')$ shown in Fig. 1 *A*; the corresponding one-dimensional probability distribution $\rho_o(\xi)$, calculated analytically, is shown in Fig. 1 *B* (*gray*). We aim to sample instead a hypothetical experimental distribution $\rho_{\exp}(\xi)$, also shown in Fig. 1 *B* (*black*). We thus carry out an overdamped Langevin dynamics simulation on the $U(\xi,\xi')$ potential, using EBMetaD to slowly construct the biasing potential $V(\xi,t)$ defined in Eq. 4. As Fig. 1 *B* shows, the calculated histogram $\rho_{\text{sim}}(\xi)$ evolves gradually until it converges to the target probability distribution. Thereafter, the simulation reaches a stationary condition, and neither $\rho_{\text{sim}}(\xi)$ nor the average bias potential change significantly (Fig. 1 *B*, *inset*). To assess whether the ensemble sampled at convergence corresponds to that defined in Eq. 3, i.e., whether EBMetaD indeed fulfills the maximum-entropy principle, we directly compare the calculated simulation histogram $\rho_{\text{sim}}(\xi,\xi')$ with the modified two-dimensional potential, $U(\xi,\xi') - \ln\rho_{\exp}(\xi) - F(\xi)$, calculated analytically ($k_BT = 1$). As Fig. 1 *C* shows, these distributions match perfectly; that is, the bias introduced so as to reproduce $\rho_{\exp}(\xi)$ does not alter $\rho(\xi')$ for any ξ-value. An extension of this test in which two hypothetical distributions $\rho_{\exp}(\xi)$ and $\rho'_{\exp}(\xi')$ are concurrently targeted further confirms that EBMetaD fulfills the maximum-entropy condition (see Appendix S3 and Fig. S2 in the Supporting Material).

To test EBMetaD in a realistic application, we next considered T4 lysozyme in explicit water (Fig. 2 *A*, and Weaver and Matthews (13)). Following Roux and Islam (4), three methanethio-sulfonate spin-labels were attached at positions E62C, T109C, and A134C. Experimental distance distributions for each pair of nitroxide groups were obtained via electron spin resonance (ESR)/DEER spectroscopy; data were kindly provided by R. A. Stein and H. S. McHaourab (Vanderbilt University Medical Center, Nashville, TN).

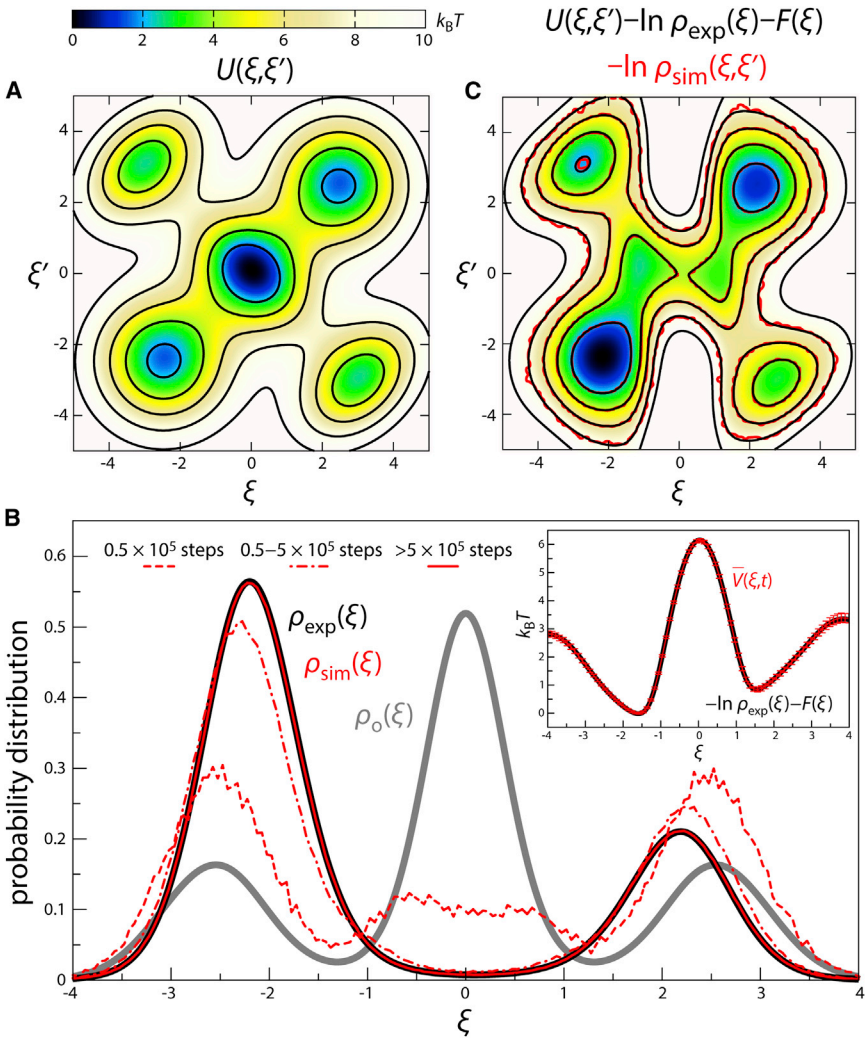

FIGURE 1 (***A***) **Model two-dimensional potential used to test EBMetaD, via an overdamped Langevin dynamics simulation. (*B*) Histogram of ξ as a function of the number of simulation steps (*red lines*), compared with the probability distribution associated with the model potential (*gray*), and with the target distribution (*black*). (*Inset*) Average biasing potential, versus $-\ln \rho_{exp}(\xi) - F(\xi)$ (Eq. 6), with $t_e = 5 \times 10^5$ steps. $F(\xi)$ was calculated analytically, as $F(\xi) = -\ln[\int d\xi' \exp\{-U(\xi,\xi')\}] + C$. (*C*) Histogram of ξ and ξ' from EBMetaD (*red isolines*), overlaid on the ensemble-corrected potential calculated analytically (*black isolines*) (Eq. 3). Diffusion coefficients in ξ,ξ' were set to 10, the integration time step was 10^{-5}, and $k_BT = 1$. Gaussians of height 10^{-4} k_BT and width 0.1 were added every 10^3 steps. Equivalent results were obtained for a wide range of alternative values (Fig. S1).**

A single trajectory of ~200 ns was then calculated with EBMetaD, using a three-dimensional biasing potential identical to that defined in Eq. 7, i.e., the three experimental distributions are targeted concurrently. For comparison, an unbiased ~270-ns trajectory was also calculated using a standard MD. As shown in Fig. 2 *B*, the distance histograms derived from the unbiased trajectory fail to reproduce those obtained experimentally. By contrast, the histograms

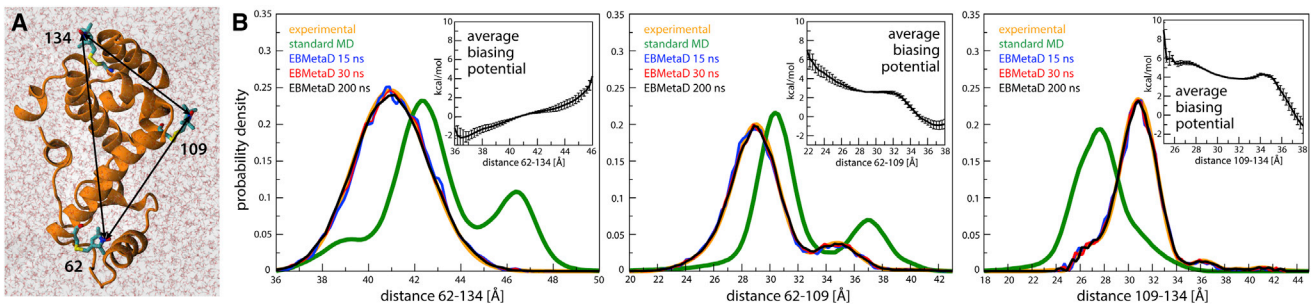

FIGURE 2 (***A***) **Spin-labeled T4 lysozyme simulated in explicit water (PDB:2LZM (13)). The protein is enclosed in a truncated-octahedron periodic box containing 11,895 TIP3P water molecules and 10 Cl^- counterions that neutralize the total charge of the system. The distances between the spin-label nitroxide groups measured by ESR/DEER are indicated (*solid arrows*). (*B*) Comparison of the experimental and calculated probability distributions for each of the spin-label pairs, from either unbiased MD simulations or EBMetaD; the latter are given for different simulation times. (*Insets*) EBMetaD biasing potential, averaged over the simulated trajectory ($t_e = 5$ ns). Error bars are standard errors over three simulation fragments (see Fig. S4 for further details).**

derived from the EBMetaD simulation converge to the ESR/DEER data within a few tens of nanoseconds, and preserve that agreement thereafter. To further assess the performance of the method, we compared the time-averaged biasing potential applied to each of the spin-spin distances in three fragments of the EBMetaD trajectory (excluding only the first 5 ns). As shown in Fig. 2 *B* (*insets*), the shape of the biasing potentials is largely constant in time, with fluctuations significantly larger than k_BT only in the distal, low-probability regions, thus confirming that EBMetaD reaches an approximately stationary condition (Eqs. 5 and 6). Consistent with the maximum-entropy principle, the ensemble correction introduced by EBMetaD primarily entails a population shift in the rotameric states of the spin labels (Fig. S3 *A*), with no significant changes in the protein backbone (Fig. S3 *B*); the root-mean-square deviation of the Cα-trace, relative to the starting x-ray structure, is within 2 Å in both the unbiased and EBMetaD trajectories.

In summary, we have introduced an enhanced-sampling MD simulation method to generate molecular ensembles that reproduce probability distributions for one or more independent observables. This method, referred to as ensemble-biased metadynamics, adaptively provides an ensemble correction consistent with the maximum entropy principle (2–6), without mean field approximations (4), multiple simulation replicas (4,5,7), or the iterative optimization of Lagrangian parameters (2,3). Owing to the computational efficiency and practical simplicity of the method, we posit that EBMetaD can be extremely useful in a wide range of applications, such as structure refinement, mechanistic studies based on spectroscopic data, or purely computational simulation studies. EBMetaD is integrated within the PLUMED 1.3 plug-in (14), and can be thus readily used with multiple simulation engines.

SUPPORTING MATERIAL

Three appendices, Supporting Materials and Methods, and four figures are available at http://www.biophysj.org/biophysj/supplemental/S0006-3495(15)00536-6.

AUTHOR CONTRIBUTIONS

F.M. and J.D.F.G. designed research and wrote the article. F.M. performed research, contributed analytical tools, and analyzed the data.

ACKNOWLEDGMENTS

This work was funded by the Division of Intramural Research of the National, Heart, Lung and Blood Institute, National Institutes of Health, Bethesda, MD.

REFERENCES

1. Jeschke, G. 2012. DEER distance measurements on proteins. *Annu. Rev. Phys. Chem.* 63:419–446.
2. Pitera, J. W., and J. D. Chodera. 2012. On the use of experimental observations to bias simulated ensembles. *J. Chem. Theory Comput.* 8:3445–3451.
3. White, A. D., and G. A. Voth. 2014. Efficient and minimal method to bias molecular simulations with experimental data. *J. Chem. Theory Comput.* 10:3023–3030.
4. Roux, B., and S. M. Islam. 2013. Restrained-ensemble molecular dynamics simulations based on distance histograms from double electron-electron resonance spectroscopy. *J. Phys. Chem. B.* 117:4733–4739.
5. Cavalli, A., C. Camilloni, and M. Vendruscolo. 2013. Molecular dynamics simulations with replica-averaged structural restraints generate structural ensembles according to the maximum entropy principle. *J. Chem. Phys.* 138:094112.
6. Roux, B., and J. Weare. 2013. On the statistical equivalence of restrained-ensemble simulations with the maximum entropy method. *J. Chem. Phys.* 138:084107.
7. Islam, S. M., R. A. Stein, …, B. Roux. 2013. Structural refinement from restrained-ensemble simulations based on EPR/DEER data: application to T4 lysozyme. *J. Phys. Chem. B.* 117:4740–4754.
8. Laio, A., and F. L. Gervasio. 2008. Metadynamics: a method to simulate rare events and reconstruct the free energy in biophysics, chemistry and material science. *Rep. Prog. Phys.* 71:126601.
9. Laio, A., and M. Parrinello. 2002. Escaping free-energy minima. *Proc. Natl. Acad. Sci. USA.* 99:12562–12566.
10. Bussi, G., A. Laio, and M. Parrinello. 2006. Equilibrium free energies from nonequilibrium metadynamics. *Phys. Rev. Lett.* 96:090601.
11. Barducci, A., G. Bussi, and M. Parrinello. 2008. Well-tempered metadynamics: a smoothly converging and tunable free-energy method. *Phys. Rev. Lett.* 100:020603.
12. Dama, J. F., M. Parrinello, and G. A. Voth. 2014. Well-tempered metadynamics converges asymptotically. *Phys. Rev. Lett.* 112:240602.
13. Weaver, L. H., and B. W. Matthews. 1987. Structure of bacteriophage T4 lysozyme refined at 1.7 Å resolution. *J. Mol. Biol.* 193:189–199.
14. Bonomi, M., D. Branduardi, …, M. Parrinello. 2009. PLUMED: a portable plugin for free-energy calculations with molecular dynamics. *Comput. Phys. Commun.* 180:1961–1972.

Ensemble-Biased Metadynamics: a Molecular Simulation Method to Sample Experimental Distributions

Supporting Information

Fabrizio Marinelli[1*] and José D. Faraldo-Gómez[1*]

[1]Theoretical Molecular Biophysics Section, National Heart, Lung and Blood Institute, National Institutes of Health, Bethesda, Maryland, USA.

*Correspondence: fabrizio.marinelli@nih.gov or jose.faraldo@nih.gov

Appendix 1

We show that Eq. 1 and Eq. 3 (see main text) are equivalent in the limit of infinitesimally small bin intervals. We first assume that the probability distribution of the atomic coordinates $\boldsymbol{X}$ is:

$$\rho(\boldsymbol{X}) = \frac{\exp\{-\beta U(\boldsymbol{X}) + \sum_i \lambda_i h_i[\xi^{\mathrm{f}}(\boldsymbol{X})]\}}{\int d\boldsymbol{X}' \exp\{-\beta U(\boldsymbol{X}') + \sum_i \lambda_i h_i[\xi^{\mathrm{f}}(\boldsymbol{X}')]\}} \quad \text{(Eq. 1)}$$

From this equation, the probability distribution of ξ can be obtained by integrating $\rho(\boldsymbol{X})$ for a fixed value of ξ:

$$\rho'(\xi) = \int d\boldsymbol{X} \rho(\boldsymbol{X}) \delta[\xi - \xi(\boldsymbol{X})] = \frac{\exp\{-\beta F(\xi) + \sum_i \lambda_i h_i(\xi)\}}{\int d\xi' \exp\{-\beta F(\xi') + \sum_i \lambda_i h_i(\xi')\}} \quad \text{(Eq. S1)}$$

By definition, the parameters λ_i in Eq. 1 are those that ensure that $\rho'(\xi) \approx \rho_{\underline{\exp}}(\xi)$; therefore, from Eq. S1 we obtain:

$$\exp\left\{\sum_i \lambda_i h_i(\xi)\right\} = Z \exp\{\ln \rho_{\exp}(\xi) + \beta F(\xi)\} \quad \text{(Eq. S2)}$$

where Z is defined as:

$$Z = \int d\xi' \exp\{-\beta F(\xi') + \sum_i \lambda_i h_i(\xi')\} \quad \text{(Eq. S3)}$$

Taken together, these expressions lead to Eq. 3:

$$\rho(\boldsymbol{X}) = \frac{\exp\{-\beta U(\boldsymbol{X}) + \ln \rho_{\exp}[\xi^{\mathrm{f}}(\boldsymbol{X})] + \beta F[\xi^{\mathrm{f}}(\boldsymbol{X})]\}}{\int d\boldsymbol{X}' \exp\{-\beta U(\boldsymbol{X}') + \ln \rho_{\exp}[\xi^{\mathrm{f}}(\boldsymbol{X}')] + \beta F[\xi^{\mathrm{f}}(\boldsymbol{X}')]\}} \quad \text{(Eq. 3)}$$

Appendix 2

We show that if both w/τ and σ are sufficiently small, the biasing potential constructed in the EBMetaD simulation fulfills Eq. 5, that is:

$$\dot{V}(\xi,t>t_e)\approx\frac{C}{\rho_{\exp}(\xi)}\frac{\exp\{-\beta[F(\xi)+V(\xi,t)]\}}{\int d\xi'\exp\{-\beta[F(\xi')+V(\xi',t)]\}}\approx C \quad \text{(Eq. 5)}$$

Let us assume that $N(t,\ \Delta t)$ is the total number of Gaussians added from time t to $t+\Delta t$, and that $n(\xi,\ t,\ \Delta t)d\xi$ is the number of Gaussians specifically added in the interval $d\xi$ around ξ in the same time-window. The distribution of ξ in this time-window can be written as:

$$\rho_{\text{EBMetaD}}(\xi,t,\Delta t)=n(\xi,t,\Delta t)/N(t,\Delta t) \quad \text{(Eq. S4)}$$

Based on this equation, the change in the EBMetaD biasing potential from time t to $t+\Delta t$ is:

$$V(\xi,t+\Delta t)-V(\xi,t)=\frac{w}{\exp\{S_\rho\}}\int d\xi'\frac{n(\xi',t,\Delta t)}{\rho_{\exp}(\xi')}\exp\left\{-[\xi-\xi']^2/2\sigma^2\right\} \quad \text{(Eq. S5)}$$

If σ is small enough, the Gaussians approximate Dirac delta functions and Eq. S5 can be written as:

$$V(\xi,t+\Delta t)-V(\xi,t)\approx\frac{w\sqrt{2\pi\sigma^2}}{\exp\{S_\rho\}}\frac{n(\xi,t,\Delta t)}{\rho_{\exp}(\xi)}=\frac{wN(t,\Delta t)\sqrt{2\pi\sigma^2}}{\exp\{S_\rho\}}\frac{\rho_{\text{EBMetaD}}(\xi,t,\Delta t)}{\rho_{\exp}(\xi)} \quad \text{(Eq. S6)}$$

We now make the additional assumption that if w/τ is sufficiently small, the shape of the bias potential does not change significantly after a certain equilibration time t_e, and therefore:

$$\rho_{\text{EBMetaD}}(\xi,t>t_e,\Delta t)\propto\exp\{-\beta[F(\xi)+V(\xi,t)\} \quad \text{(Eq. S7)}$$

Under this hypothesis, if we divide Eq. S6 by Δt we obtain an expression analogous to Eq. 5:

$$\dot{V}(\xi,t>t_e)\approx\frac{w\sqrt{2\pi\sigma^2}}{\tau\exp\{S_\rho\}\rho_{\exp}(\xi)}\frac{\exp\{-\beta[F(\xi)+V(\xi,t)]\}}{\int d\xi'\exp\{-\beta[F(\xi')+V(\xi',t)]\}}\approx\frac{w\sqrt{2\pi\sigma^2}}{\tau\exp\{S_\rho\}} \quad \text{(Eq. S8)}$$

The condition that w/τ is small implies that the EBMetaD simulation remains close to equilibrium. Similarly to Metadynamics, this condition can be explicitly imposed by gradually reducing w/τ throughout the simulation (1-3). In practice, EBMetaD converges reasonably well as long as w/τ is such that significant variations in the shape of the biasing potential acting on ξ (say, of a few k_BT) are slower than the equilibration time of any degree of freedom orthogonal to ξ(4-6). An indication of convergence after the initial equilibration stage is an even growth of the biasing potential along ξ (Eq. S8). This equilibration time could be accelerated as in other Metadynamics variants (4), for example using a bias-exchange multi-replica scheme (7). In complex systems it is conceivable that the sampling of the observables for which an experimental distribution is known is hampered by other slow degrees of freedom in the system. In Bias-Exchange Metadynamics (7), independent simulations that apply a bias to different reaction coordinates can be coupled by Metropolis Monte-Carlo exchanges, as in Hamiltonian replica-exchange. In problematic cases, therefore, a

conventional Metadynamics bias could be used in a subset of replicas in order to enhance the reversible exploration of those slow degrees of freedom, while a different replica (or replicas) would utilize the EBMetaD method to reproduce a specific probability distribution.

If the biased variables include the slow degrees of freedom, EBMetaD displays similar features of standard Metadynamics (4-6); that is, the biased probability distribution converges to the experimental histogram as the average biasing potential converges to Eq. 6, for a wide range of possible simulation parameters (see Fig. S1). The instantaneous biasing potential, however, will fluctuate around the average, again as in conventional Metadynamics, to a degree that depends on the parameters defining the biasing potential. This fluctuation range can be described with good accuracy by the following expression (8):

$$\bar{\varepsilon} = \int d\xi\, \varepsilon(\xi,t)\rho_{\exp}(\xi) = C\sqrt{\frac{w\tau_S\sigma}{\tau\beta\exp\{S_\rho\}}} \quad \text{(Eq. S9)}$$

where $\varepsilon(\xi,t)$ is the instantaneous error in the bias potential, defined as:

$$\varepsilon(\xi,t) = \sqrt{\left\langle \left[V(\xi,t) - \left\langle V(\xi,t)\right\rangle\right]^2 \right\rangle} \quad \text{(Eq. S10)}$$

In Eq. S9, τ_S is a relaxation time that depends on the target distribution. For unimodal distributions, $\tau_S \sim [\exp\{S\rho\}]^2/D$, where D is the diffusion coefficient of observable ξ. However, multiple peaks in the target distribution (i.e. free-energy barriers imposed by the bias) imply a larger value of τ_S. For the model systems investigated in this study and the range of parameters explored (Figs. S1), Eq. S9 is fulfilled with $C \sim 0.7$ (Fig. S1E). Eq. S9 can be used to initially select the simulation parameters as in standard Metadynamics, i.e. σ can be selected to match the desired spatial resolution, and w/τ can be tuned so that the average error is in the order of $k_B T$.

Appendix 3

The maximum entropy principle can be easily generalized to multiple observables ξ_j and probability distributions $\rho_{\exp}(\xi_j)$ as a sum the linear perturbations induced separately by each histogram:

$$\rho(\boldsymbol{X}) = \frac{\exp\{-\beta U(\boldsymbol{X}) + \sum_{ij}\lambda_{ij}h_{ij}[\xi_j^{\mathrm{f}}(\boldsymbol{X})]\}}{\int d\boldsymbol{X}'\exp\{-\beta U(\boldsymbol{X}') + \sum_{ij}\lambda_{ij}h_{ij}[\xi_j^{\mathrm{f}}(\boldsymbol{X}')]\}} \quad \text{(Eq. S11)}$$

Similarly to the one-dimensional case, $h_{ij}[\xi_j^{\mathrm{f}}(\boldsymbol{X})] = 1$ if $\xi_j^{\mathrm{f}}(\boldsymbol{X})$ is in bin i and 0 otherwise, and the λ_{ij} parameters ensure that the time averages of $h_{ij}[\xi_j^{\mathrm{f}}(\boldsymbol{X})]$ are equal to the experimental probability values. Also in this case, Eq. S11 can be written in terms of free energies and target probability distributions. Selecting the observable ξ_k and integrating Eq. S11 for a fixed value of ξ_k we obtain:

$$\rho'(\xi_k) = \int d\boldsymbol{X}\rho(\boldsymbol{X})\delta(\xi_k - \xi_k^{\mathrm{f}}(\boldsymbol{X})) = \frac{\exp\{-\beta F_{\mathrm{e}}(\xi_k) + \sum_i \lambda_{ik}h_{ik}\xi_k\}}{\int d\xi_k'\exp\{-\beta F_{\mathrm{e}}(\xi_k') + \sum_i \lambda_{ik}h_{ik}\xi_k'\}} \quad \text{(Eq. S12)}$$

where $F_e(\xi_k)$ is the free energy along ξ_k after the ensemble has been corrected along the other observables $\xi_{j\neq k}$:

$$F_e(\xi_k) = -\frac{1}{\beta}\ln\int d\boldsymbol{X}\,\delta(\xi_k - \xi_k^f(\boldsymbol{X}))\,\exp\{-\beta U(\boldsymbol{X}) + \sum_{i,j\neq k}\lambda_{ij}h_{ij}[\xi_j^f(\boldsymbol{X})]\} \quad \text{(Eq. S13)}$$

As mentioned, the parameters λ_{ij} in Eq. S11 are by definition those that ensure $\rho'(\xi_k) = \rho_{exp}(\xi_k)$; therefore we obtain:

$$\rho(\boldsymbol{X}) = \frac{\exp\{-\beta U(\boldsymbol{X}) + \sum_j \ln(\rho_{exp}[\xi_j^f(\boldsymbol{X})]) + \sum_j \beta F_e[\xi_j^f(\boldsymbol{X})]\}}{\int d\boldsymbol{X}'\exp\{-\beta U(\boldsymbol{X}') + \sum_j \ln(\rho_{exp}[\xi_j^f(\boldsymbol{X}')]) + \sum_j \beta F_e[\xi_j^f(\boldsymbol{X}')]\}} \quad \text{(Eq. S14)}$$

Analogously the free energies $F_e(\xi_k)$ can be defined as:

$$F_e(\xi_k) = -\frac{1}{\beta}\ln\int d\boldsymbol{X}\,\delta(\xi_k - \xi_k^f(\boldsymbol{X}))\,\exp\{-\beta U(\boldsymbol{X}) + \sum_{j\neq k}\ln(\rho_{exp}[\xi_j^f(\boldsymbol{X})]) + \sum_{j\neq k}\beta F_e[\xi_j^f(\boldsymbol{X})]\} \quad \text{(Eq. S15)}$$

In practice, in EBMetaD the multi-dimensional ensemble correction is provided by a sum of biasing potentials for each observable:

$$V(\xi_1,\xi_2,\ldots,t) = \sum_j V(\xi_j,t) = \sum_j \sum_{t'=\tau,2\tau\ldots}^{t} \frac{w_j \exp\left\{-[\xi_j - \xi_j^f(\boldsymbol{X}_{t'})]^2 / 2\sigma_j^2\right\}}{\exp\{S_{\rho_j}\}\rho_{exp}[\xi_j^f(\boldsymbol{X}_{t'})]} \quad \text{(Eq. S16)}$$

That is, several one-dimensional biasing potentials are constructed concurrently, rather than a single multi-dimensional potential (as in standard Metadynamics), which results in faster convergence (9). Similarly to the one dimensional case, if w_j/τ is sufficiently small, for $t > t_e$ the simulation reaches a stationary condition in which the instantaneous biasing potential oscillates around the theoretical profile expected from the maximum-entropy principle (Eq. S14), and thus the distribution along each observable matches the target probability density, that is:

$$\bar{V}(\xi_j, t > t_e) \approx -\frac{1}{\beta}\ln(\rho_{exp}[\xi_j^f(\boldsymbol{X})]) - F_e[\xi_j^f(\boldsymbol{X})] \quad \text{(Eq. S17)}$$

Supplementary Methods

Langevin Dynamics simulations – The functional form of the potential in Fig. 1A and Fig. S2A is:

$$
\begin{aligned}
U(\xi,\xi') = \; & -11.4\times\exp\left\{-\frac{1}{2}\left[\frac{\xi+\xi'}{\sqrt{2}}\right]^2\right\}\exp\left\{-\frac{1}{2\times1.5^2}\left[\frac{\xi-\xi'}{\sqrt{2}}\right]^2\right\} \\
& -11.4\times\exp\left\{-\frac{1}{2\times1.5^2}\left[\frac{\xi+\xi'}{\sqrt{2}}-3.5\right]^2\right\}\exp\left\{-\frac{1}{2\times1.5^2}\left[\frac{\xi-\xi'}{\sqrt{2}}\right]^2\right\} \\
& -10.2\times\exp\left\{-\frac{1}{2\times1.5^2}\left[\frac{\xi+\xi'}{\sqrt{2}}\right]^2\right\}\exp\left\{-\frac{1}{2}\left[\frac{\xi-\xi'}{\sqrt{2}}-4.3\right]^2\right\} \\
& -10.2\times\exp\left\{-\frac{1}{2\times1.5^2}\left[\frac{\xi+\xi'}{\sqrt{2}}\right]^2\right\}\exp\left\{-\frac{1}{2}\left[\frac{\xi-\xi'}{\sqrt{2}}+4.3\right]^2\right\} \\
& -11.4\times\exp\left\{-\frac{1}{2\times1.5^2}\left[\frac{\xi+\xi'}{\sqrt{2}}+3.5\right]^2\right\}\exp\left\{-\frac{1}{2\times1.5^2}\left[\frac{\xi-\xi'}{\sqrt{2}}\right]^2\right\}
\end{aligned}
$$

Molecular Dynamics simulations – The simulations of T4 lysozyme were carried out with NAMD 2.9 (10) and a modified version of PLUMED (9) that implements EBMetaD. We used the CHARMM27/CMAP (11,12) forcefield for the protein and solvent, and the parameters of Sezer et al. (13) for the spin-labels. The simulations were carried out at constant temperature (298 K) and pressure (1 atm) using periodic boundary conditions in all directions, and a time-step of 2 fs. Electrostatic interactions were calculated using Particle-Mesh-Ewald with a real-space cut-off of 12 Å; the same cut-off distance was used for van der Waals interactions. The variables considered in the EBMetaD simulations were the pairwise distances between the centers of mass of the nitroxide groups in the spin-labels. Gaussians of height 0.05 kcal/mol and width 0.5 Å were added every 2 ps (i.e. every 10^3 steps), and scaled by the experimental probability distributions according to Eq. 7 (see main text). This height was selected on the basis of Eq. S9, so that the average error of the average biasing potential is in the order of k_BT. To evaluate Eq. S9, we considered $\tau_S \sim [\exp\{S\rho\}]^2/D$ and $D \sim 0.1$ Å^2/ps was estimated from the standard MD simulation as the initial slope of the mean-square displacement of the spin-label distances (e.g. $D \sim 0.05$ Å^2/ps for the 62-134 pair). The standard deviation of the biasing potential around the average, calculated *a posteriori* via Eq. S10 is in good agreement with the initial estimate (based on Eq. S9), namely 1.5 k_BT, 2 k_BT and k_BT for spin-label pairs 62-109, 62-134 and 109-134, respectively.

Supplementary Figures

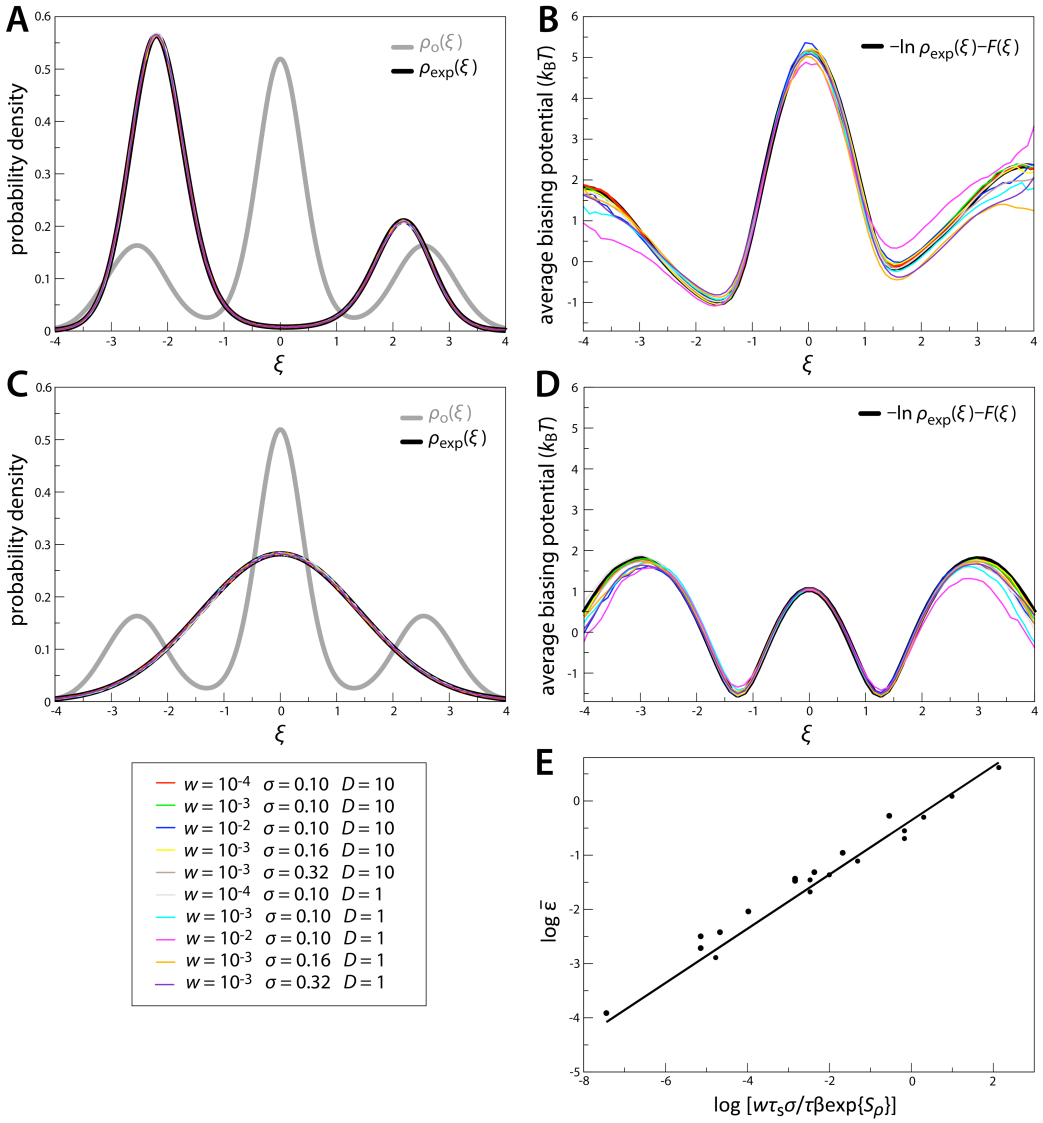

Figure S1. Robustness of the EBMetaD method against variations in the parameters defining the biasing potential (Eq. 4), for the model 2D potential shown in Fig. 1. **(A)** Bi-modal target probability distributions $\rho_{exp}(\xi)$ (black) compared with the distributions obtained with EBMetaD simulations (colored lines), for different values of the nominal height and width of the biasing Gaussians, w and σ, respectively, and for different values of the diffusion constant, D. (**B**) The average biasing potential resulting from the EBMetaD simulations (colored lines) is compared with the theoretical results, calculated analytically (see caption of Fig. 1). (**C**, **D**) Same as (A, B), for a unimodal target probability distribution. (**E**) Error in the average biasing potential as a function of the EBMetaD simulation parameters demonstrates validity of Eq. S9. For the target distribution shown in panel (B), we used $\tau_S \sim [\exp\{S\rho\}]^2/D$, while for that in panel (A), τ_S was scaled by an Arrhenius factor on account of the free energy barrier, i.e. $\tau_S \sim 20\ [\exp\{S\rho\}]^2/D$. The data fulfills the linear relationship in Eq. S9 with $C \sim 0.7$.

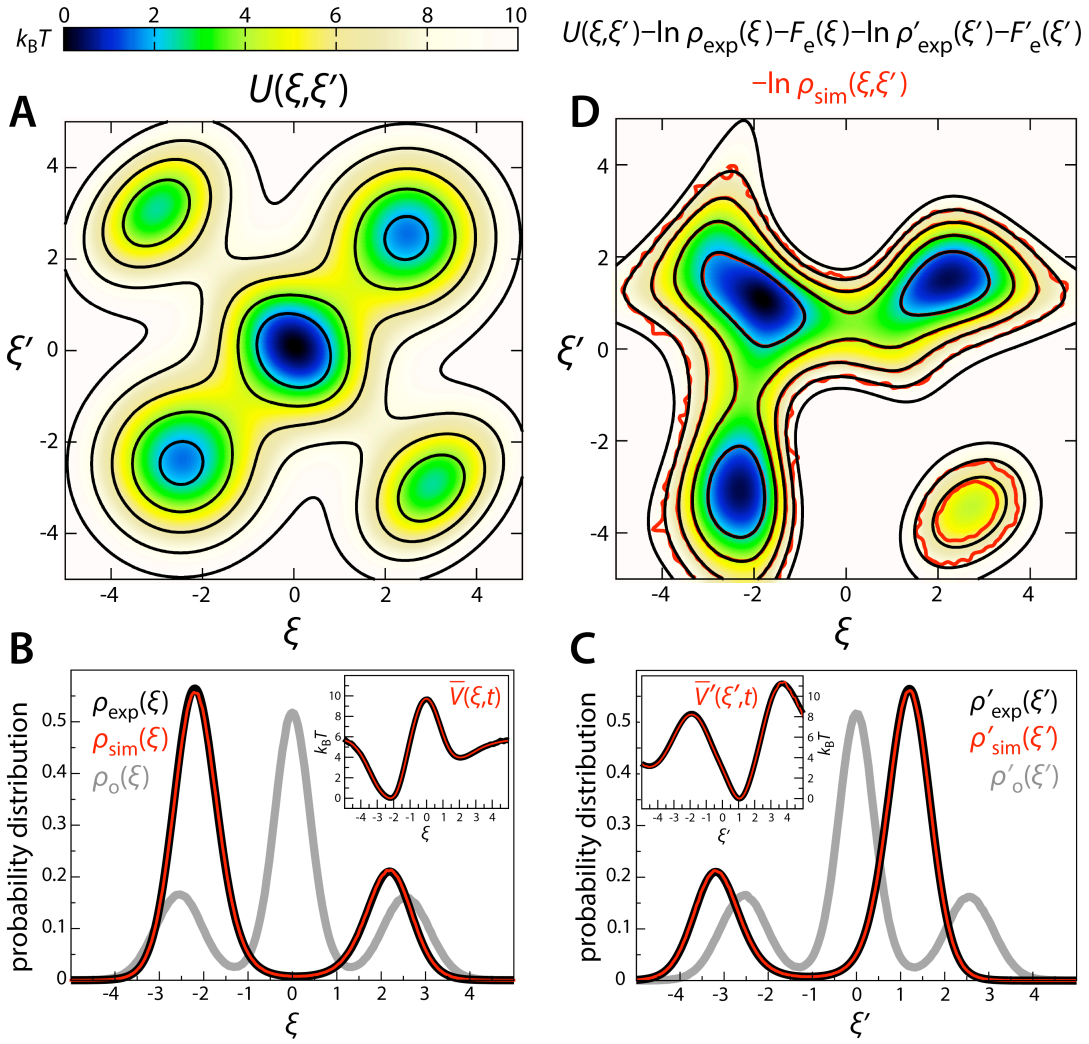

Figure S2. (**A**) Model 2D potential used to test EBMetaD, via an overdamped Langevin dynamics simulation. (**B, C**) Histograms of ξ and ξ' calculated directly from the EBMetaD simulation (red lines), compared with the probability distributions associated with the model potential (gray), and with the target distributions (black). *Insets*: average biasing potentials in each case, compared with $-ln\ \rho_{exp}(\xi)\ -F_e(\xi)$ and $-ln\ \rho'_{exp}(\xi')\ -F'_e(\xi')$ (see Eq. S18), with $t_e = 5\times10^5$ steps. $F_e(\xi)$ and $F'_e(\xi')$ were calculated analytically (see Appendix 3). (**D**) Histogram of ξ and ξ' from the EBMetaD simulation (red isolines), overlaid on the ensemble-corrected potential calculated analytically (black isolines) (see Appendix 3). Diffusion coefficients in ξ and ξ' were set to 10, the integration time step was 10^{-5} and $k_BT = 1$. Gaussians of height 10^{-4} k_BT and width 0.1 were added to the biasing potential every 10^3 steps.

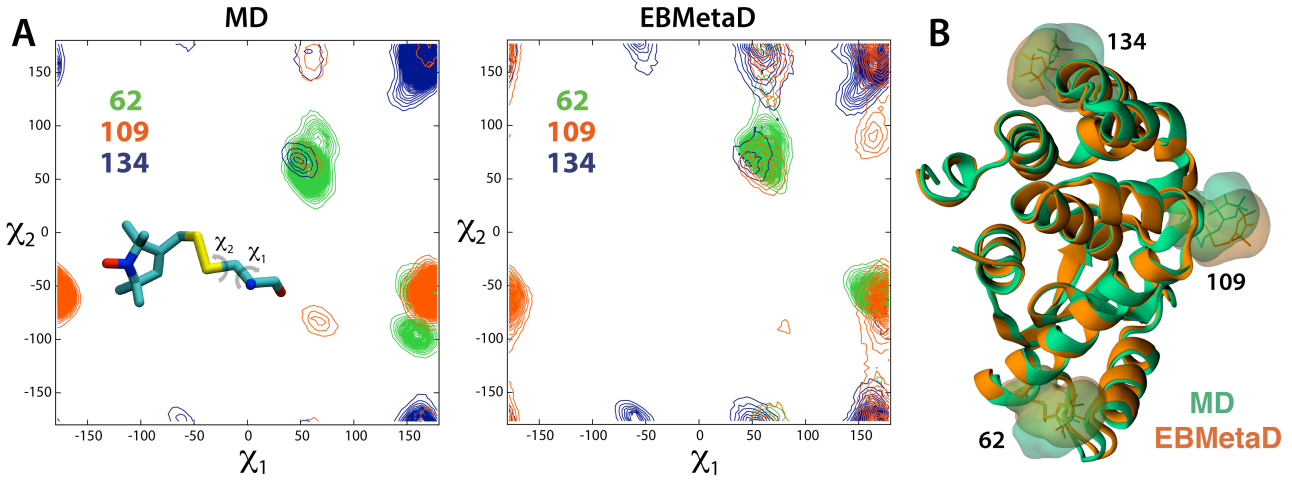

Figure S3. Rotameric configurations of the spin-labels explored in the EBMetaD and unbiased MD simulations of T4 lysozyme. (**A**) Contoured histograms of the χ_1 and χ_2 dihedral angles for each of three spin-labels (structure shown as inset). (**B**) Time-averaged backbone structure in the MD and EBMetaD trajectories, along with volume occupancy maps for each of the spin-labels.

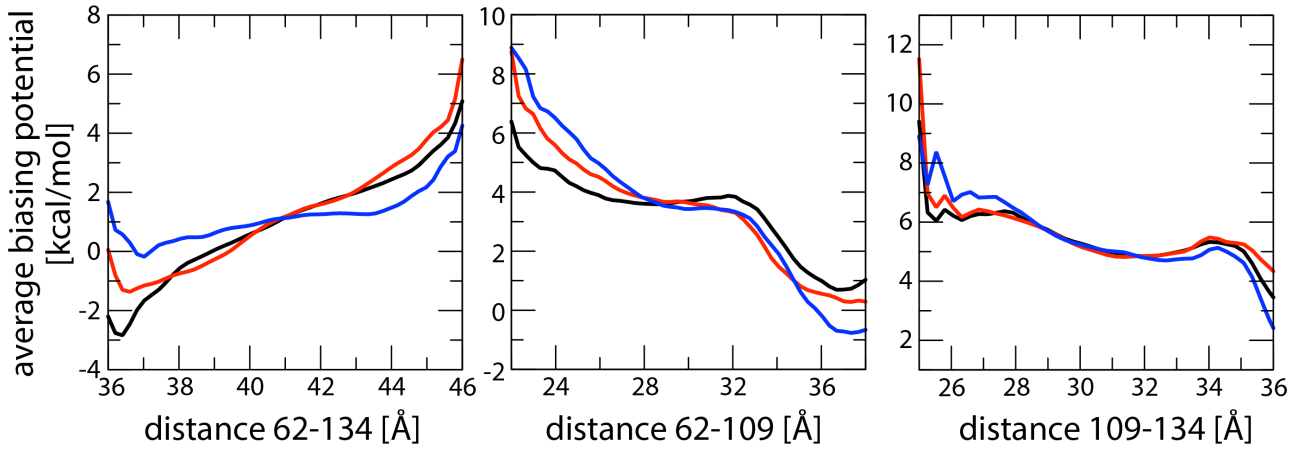

Figure S4. Time-averaged biasing potentials for each of the three spin-label distances targeted in the EBMetaD simulations of T4 lysozyme, for three time-windows of simulation of approximately 65 ns each. If we denote these average potentials as V_1 (black), V_2 (blue), and V_3 (red), the average biasing potentials shown in the insets of Fig. 2B are $V_o = \Sigma\ V_i / N$ (N = 3), for each of the distances, while the corresponding error bars are equal to $[\Sigma\ (V_i - V_o)^2 / N\ (N\text{-}1)]^{1/2}$. Note that in order to calculate these error bars, the biasing potentials accumulated at different time-points, these potentials need to be shifted, as in the figure. Here, the instantaneous biasing potentials $V(\xi,t)$ are shifted by an offset $V_{ref}(t) = \int d\xi\ V(\xi,t)\ \rho_{exp}(\xi)$, where $\rho_{exp}(\xi)$ is the target probability distribution. The standard deviation around the average biasing potential, calculated *a posteriori* (via Eq. S10) is in good agreement with the initial theoretical estimate in Eq. S9, namely 1.5 k_BT, 2 k_BT and k_BT for spin labels 62-109, 62-134 and 109-134, respectively.

Supplementary References

1. Dama, J. F., M. Parrinello, and G. A. Voth. 2014. Well-tempered Metadynamics converges asymptotically. Phys. Rev. Lett. 112:240602.
2. Dama, J. F., G. Rotskoff, M. Parrinello, and G. A. Voth. 2014. Transition-tempered metadynamics: robust, convergent Metadynamics via on-the-fly transition barrier estimation. J. Chem. Theor. Comp. 10:3626-3633.
3. Barducci, A., G. Bussi, and M. Parrinello. 2008. Well-tempered metadynamics: a smoothly converging and tunable free-energy method. Phys. Rev. Lett. 100:020603.
4. Laio, A. and F. L. Gervasio. 2008. Metadynamics: a method to simulate rare events and reconstruct the free energy in biophysics, chemistry and material science. Rep. Prog. Phys. 71:126601.
5. Crespo, Y., F. Marinelli, F. Pietrucci, and A. Laio. 2010. Metadynamics convergence law in a multidimensional system. Phys. Rev. E 81:055701.
6. Bussi, G., A. Laio, and M. Parrinello. 2006. Equilibrium free energies from nonequilibrium metadynamics. Phys. Rev. Lett. 96:090601.
7. Piana, S. and A. Laio. 2007. A bias-exchange approach to protein folding. J. Phys. Chem. B 111:4553-4559.
8. Laio, A., A. Rodriguez-Fortea, F. L. Gervasio, M. Ceccarelli, and M. Parrinello. 2005. Assessing the accuracy of metadynamics. J. Phys. Chem. B 109:6714-6721.
9. Gil-Ley, A. and G. Bussi. 2015. Enhanced conformational sampling using replica exchange with collective-variable tempering. J. Chem. Theor. Comp. 11:1077-1085.
10. Phillips, J. C., R. Braun, W. Wang, J. Gumbart, E. Tajkhorshid, E. Villa, … K. Schulten. 2005. Scalable molecular dynamics with NAMD. J. Comp. Chem. 26:1781-1802.
11. MacKerell, A. D., D. Bashford, M. Bellott, R. L. Dunbrack, J. D. Evanseck, M. J. Field, … M. Karplus. 1998. All-atom empirical potential for molecular modeling and dynamics studies of proteins. J. Phys. Chem. B 102:3586-3616.
12. Mackerell, A. D., M. Feig, and C. L. Brooks. 2004. Extending the treatment of backbone energetics in protein force fields: Limitations of gas-phase quantum mechanics in reproducing protein conformational distributions in molecular dynamics simulations. J. Comp. Chem 25:1400-1415.
13. Sezer, D., J. H. Freed, and B. Roux. 2008. Parametrization, molecular dynamics simulation, and calculation of electron spin resonance spectra of a nitroxide spin label on a polyalanine alpha-helix. J. Phys. Chem. B 112:5755-5767.